A Reservoir Computer Approach for Data-driven Reconstruction of Insect Locomotion Nonlinear Dynamics for Bioacoustics Applications

Omid Sedehi (1), Merten Stender (2), Joseph C. S. Lai (3), and Sebastian Oberst (1)

(1) Centre for Audio, Acoustics and Vibration (CAAV), School of Mechanical and Mechatronic Engineering, University of Technology Sydney, Ultimo, NSW 2007, Australia
(2) Chair of Cyber-Physical Systems in Mechanical Engineering, Technosphere Universität Berlin, Straße des 17. Juni 135, 10623 Berlin, Germany
(3) School of Engineering and Technology, University of New South Wales, Northcott Dr, Canberra, ACT, 2612, Australia

ABSTRACT

Data-driven identification and reconstruction of vibroacoustic signals receive extensive interest in studying insects' locomotion mechanisms for bioacoustics and robotics applications. However, the nonlinearity and complexity of locomotion dynamics challenge the recovery of the governing equations when handling noisy measurements. Reservoir computing is regarded as a class of recurrent neural networks inspired by the structure of the human brain, consisting of a set of neurons and randomly selected synapses that efficiently operate on different learning tasks. It has emerged as an efficient and interpretable tool for identifying and representing nonlinear dynamics in a grey-box fashion without requiring sparsity constraints over a pre-selected library of basis functions. Along this direction, this study presents results on a novel reservoir computing framework for implicitly discovering the governing equations from input-output data driven from simulations of insect locomotion dynamics. It also provides insights on the calibration of reservoir hyperparameters and visualises the search domain for prediction tasks. It further compares the validation accuracy of computer reservoirs when dealing with additive deterministic noise. From the results demonstrated on numerical examples, it is concluded that reservoir computers can provide competitive performance, offering good efficiency and accuracy subject to appropriate hyperparameter calibration and pruning redundant neurons and synapses.

1 INTRODUCTION

Simulation of multi-legged arthropod locomotion is crucial for understanding and implementing bio-inspired gait mechanisms for energy-efficient robotics applications (Full et al., 1990; Seidl et al., 2008; Reinhardt et al., 2009). Such motions include walking, trotting, and running/hopping movements, with and without extended flight stages, shaped through millions of years of evolution and creating unique and distinct locomotion dynamics among different species, showing enormous variability in the number of legs, leg length, leg shape, leg position, and body mass distribution across legs (Blickhan et al., 1993). Despite natural diversity, the literature suggests using simple mass-spring-based dynamic systems, such as inverted pendulum-based systems and bouncing gaits, to simulate complex dynamics (Full et al., 1991; Gan et al., 2018). While inverted pendulum models are suited to simulate walking mechanics, the Spring-Loaded Inverted Pendulum (SLIP) is well recognised for describing running mechanisms (Geyer et al., 2006; Pelit et al., 2020). Although these models were initially proposed to mimic human walking and running motions, recent works show significant similarities between the walking mechanism of humans and arthropods, and such simplified models appear to remain valid and relevant (Blickhan et al., 1993; Geyer et al., 2006). A bipedal SLIP dynamic model has recently been utilised to simulate all common bipedal gaits when the initial conditions are carefully adjusted (Gan et al., 2018). Then, the solution of the Poincaré map equation provides different periodic orbits, characterising physically reasonable motions from different branches of the bifurcation diagram (Gan et al., 2018). Despite these advances, the complexity and nonlinearity of locomotion dynamics create hurdles for efficiently regenerating physical motions, especially when hardware implementation is desirable.

Replicating arthropods' locomotion has also unveiled promising research directions in bioacoustics. Predator ground-reaction forces are used as excitation sources to generate on arbitrary substrates vibroacoustic responses, by applying the noise-control engineering principle (Oberst et al. 2019). These responses can then be

synthesised in bioacoustics applications to appear as predator cues to repel prey or prey cues to attract predators toward a desired direction (Oberst et al., 2017; Oberst et al., 2025) and used in bioassays, rather than just using playback experiments. The predator-prey relationship between ants and termites is an interesting application in this context, primarily inspired by prior research showing that termites communicate mainly through vibration (Sansom et al., 2025), eavesdrop to avoid predatory ants (Oberst et al., 2017), and assess the food quantity and quality (Evans et al., 2005; Inta et al., 2007; Oberst et al., 2017). Termites also use mud to manipulate moisture content in wood (Oberst et al., 2016; Oberst et al., 2019). Reproducing such nonlinear vibroacoustic information requires a computational framework that supports the software and hardware implementation efficiently.

Reservoir computing is a promising approach to modelling and reconstructing complex dynamics (Jaeger and Hass, 2004; Ghani et al., 2010; Throne et al., 2022). The core idea is to project the data into a high-dimensional space specified by a reservoir matrix and identify hidden features of the data for addressing specific learning tasks. This computation will take place with minimal neuronal configuration, where only the readout nodes will be trained, and the reservoir structure is fixed, considering a randomly initialised configuration. However, in most cases, a randomly initialised reservoir reduces efficiency and accuracy, and recent works have shown that reservoir computers with an optimised internal structure are crucial, especially in computationally intensive implementations (Ren and Ma, 2022; Yadav et al., 2025; Sedehi et al., 2025). Pruning reservoir neurons and synapses has recently been shown to build a sparse reservoir that enhances the prediction accuracy and reduces computational costs (Sedehi et al., 2025).

This paper is built upon our prior work of Sedehi et al. (2025), focused on truncated reservoir computing and equipped with neuronal and synaptic pruning. It explores applications to reconstruct arthropods' locomotion from partially known noisy dynamical states. For this purpose, a bipedal SLIP model is employed to generate synthetic data and validate the prediction accuracy of the truncated reservoir computer. The reservoir computer is trained and validated on the generated data, incorporating hyperparameter calibration and neuronal/synaptic pruning strategies. Vertical ground reaction forces are estimated from the centre of mass coordinates data, and insights are provided for the selection of hyperparameters and pruning when dealing with noisy data.

2 INSECT LOCOMOTION MODEL

A bipedal SLIP model has been established as a comprehensive model to describe complex insect locomotion behaviour (Geyer et al., 2006; Blickhan et al., 1993; Gan et al., 2018). Figure 1 shows a general schematic of the Bipedal SLIP model. The mass (M) represents the insect body at the coordinates (x, y) with polar mass moment of inertia J, and the mass (m) attached to the base of the springs represents the leg's mass. The uncompressed length of the springs with constant stiffness k_s is denoted by l_0, whereas the compressed length is denoted by l_1 and l_2. The rotational angle of these springs with the vertical axis is denoted by α_1 and α_2. A torsional spring with stiffness $k_\theta = ml_0^2\omega_s^2$ creates a torque between the legs, represented when the angles α_1 and α_2 deviates from the vertical stance of $\alpha_1 = \alpha_2 = 0$, with swing angular frequency of ω_s. For insects, the leg mass (m) is comparatively much smaller than the body mass (M), and the leg is very stiff too, thus the leg mass and damping are ignored $(m, d \to 0)$.

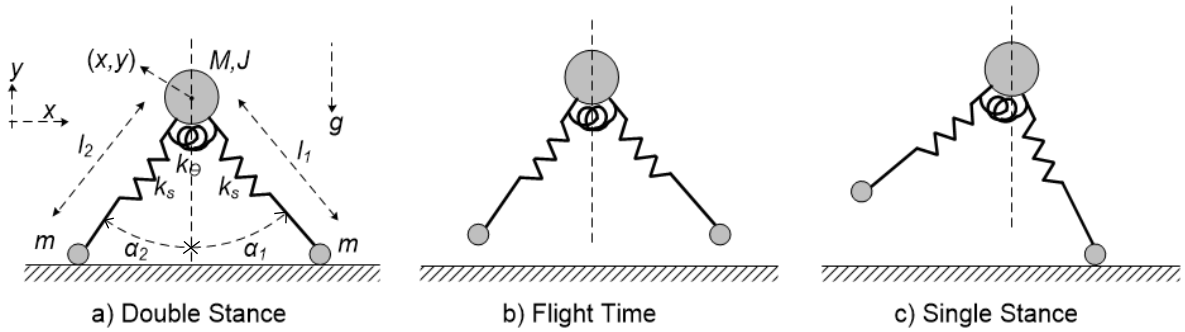

Figure 1: A schematic diagram displaying a bipedal SLIP model employed to generate periodic orbits corresponding to walking and running mechanisms. (a) Double stance position: both legs are in contact with the surface. (b) Flight time: both legs are detached from the surface, being at their uncompressed states. (c) The right leg is in contact with the surface, but the left leg is detached.

Given the above assumptions and after ignoring terms related to leg mass, the nonlinear dynamical equations governing the body movements is described by:

$$\ddot{x} = -\frac{k_s}{M}(l_0 - l_1)\sin\alpha_1 - \frac{k_s}{M}(l_0 - l_2)\sin\alpha_2 \tag{1}$$

Proceedings of ACOUSTICS 2025
12-14 November 2025,
Joondalup, Australia

$$\ddot{y} = -\frac{k_s}{M}(l_0 - l_1)\cos\alpha_1 - \frac{k_s}{M}(l_0 - l_2)\cos\alpha_2 - g \tag{2}$$

$$\ddot{\alpha_1} = -\frac{1}{l_0}(\ddot{x}\cos\alpha_1 + \ddot{y}\sin\alpha_1) - \omega_s^2\alpha_1 \tag{3}$$

$$\ddot{\alpha_2} = -\frac{1}{l_0}(\ddot{x}\cos\alpha_2 + \ddot{y}\sin\alpha_2) - \omega_s^2\alpha_1 \tag{4}$$

Although four degrees-of-freedom are involved here, i.e. x, y, α_1, α_2, only three of them are independent since the leg mass is ignored. The touch-down event happens when the mass height equals the vertical projection of leg length, and the lift-off event occurs when the leg reaches its uncompressed length. Therefore, when solving these equations for a periodic solution, zero-crossing of these two events must be checked to make the required adjustments based on the contact conditions, as shown in Figure 1.

Aiming to produce simulated data for ant locomotion, the following values are considered from the literature (Oberst et al., 2025): $M = 9.1 \times 10^{-6}$ kg, $J \to 0$, $g = 9.81$ m/s^2, $l_0 = 8$ mm, $k_s = 0.221$ N/m, and $\omega_s = 78.3$ rad/s. Based on these assumptions and specifying the initial stride according to Gan et al. (2018), the dynamical equations can be solved, and periodic orbits can be determined. This process is equivalent to finding the solutions to the Poincaré map (Ψ: $\mathbb{R}^7 \to \mathbb{R}^7$) of $\Psi(\chi^*) - \chi^* = 0$, where $\chi^* = [y, \alpha_1, \alpha_2, \dot{x}, \dot{y}, \dot{\alpha}_1, \dot{\alpha}_2]$ is the initial/final state vector in a periodic orbit that starts at $x = 0$. Depending on the initial conditions, the solution of the Poincaré map equation might land in different branches of the bifurcation diagram. Figure 2 shows the vertical ground reaction forces of the left and right legs for periodic walking and running motions. Those instants at which the reaction force is zero correspond to the detachment from the ground when the legs reach their rest length. In both walking and running motions, the motion of the right and left legs is asymmetrical, meaning that each leg is in the opposite state to the other.

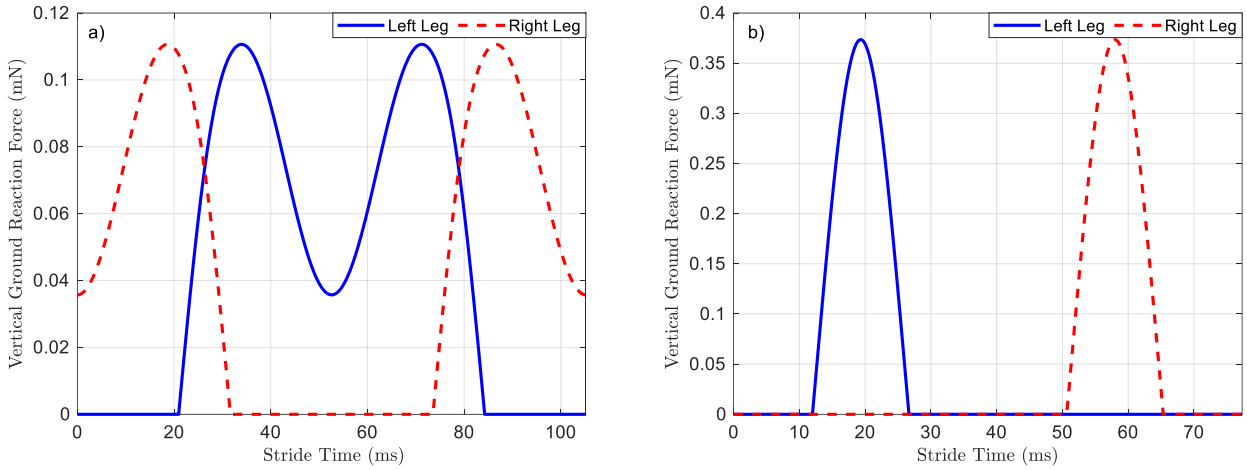

Figure 2: Ground reaction force of the left and right legs during a single stride of walking and running. (a) Walking motion is understood as an “M” shape, showing an initial stance on the right leg, followed by a double stance, and finally a single stance on the left leg. (b) Running motion is represented as a single stance on the left leg, followed by a flight interval, and finally a single stance on the right leg.

3 TRUNCATED RESERVOIR COMPUTING FRAMEWORK

In the context of reservoir computing, the Echo State Network (ESN) has widely been employed for simulating nonlinear dynamics through projecting an input vector into a high-dimensional space characterised by a “reservoir” and producing an output vector by reading from an adaptive set of readout nodes trained for specific tasks. Figure 3 shows a simple schematic of the ESN, indicating a set of neurons interconnected via random synapses, operating recursively like recurrent neural networks. The dynamical states of the ESN are described by

$$\mathbf{r}(t_i) = (1-\alpha)\mathbf{r}(t_{i-1}) + \alpha\, \mathrm{f}(\mathbf{W}_{\mathrm{res}}\mathbf{r}(t_{i-1}) + \beta\mathbf{W}_{\mathrm{in}}\mathbf{u}(t_{i-1}) + \mathbf{b}) \tag{5}$$

where $\mathbf{r}(t_i)$ is the state vector, $t_i = i\Delta t, \forall i = \{1,2,\dots,n\}$ is the discrete time index, representing time samples from Δt intervals, $\mathbf{W}_{\mathrm{res}}$ is the reservoir matrix, considered to be an Erdös–Rényi (ER) graph matrix with p internal connectivity, $\mathbf{W}_{\mathrm{in}}$ is the input-to-state projection matrix, α is the leakage rate, β is the input scaling factor, $\mathbf{b}$ is a bias vector, and $f(.)$ is an activation function, considered tangent hyperbolic function, i.e., $\tanh(.)$. By collecting n observed samples into $\mathbf{Y}_n$ and the latent states into $\mathbf{R}_n$, a ridge regression can be carried out to infer a readout matrix ($\mathbf{W}_{\mathrm{readout}}$) from minimising the following loss function:

$$L = \left\|\widehat{\mathbf{Y}}_n - \mathbf{W}_{\text{readout}}\mathbf{R}_n\right\|_2^2 + \lambda\|\mathbf{W}_{\text{readout}}\|_2^2 \tag{6}$$

where $\widehat{\boldsymbol{Y}}_n$ is a vector of actual observations, and L is the loss function regularised via the readout matrix norm multiplied by the ridge coefficient λ, giving the following explicit solution for the readout matrix:

$$\widehat{\mathbf{W}}_{\text{readout}} = (\mathbf{R}_n^T\mathbf{R}_n + \lambda\mathbf{I})^{-1}\mathbf{R}_n^T\widehat{\boldsymbol{Y}}_n \tag{7}$$

In the original formulation of the ESN, the reservoir and the input-to-state matrices are often pre-selected randomly, considering weighted Erdős–Rényi matrices. Nonetheless, recent works show great potential in optimising the reservoir computational structure by removing redundant neurons and synapses, as well as optimising hyperparameters (Sedehi et al., 2025). The present study follows the same approach to optimise the hyperparameters by further minimising the loss function for optimal values. The hyperparameters considered here include the leakage rate (α), the input scaling factor (β), the number of reservoir nodes (N), the leakage rate defined as the largest eigenvalue of the reservoir matrix ($\zeta = \max(\text{eig}(\mathbf{W}_{\text{res}}))$, and the internal connectivity rate of the reservoir matrix (p). Additionally, it employs a pruning approach to discard redundant neurons and synapses from the reservoir matrix, aiming to boost the validation accuracy and reduce the computational cost.

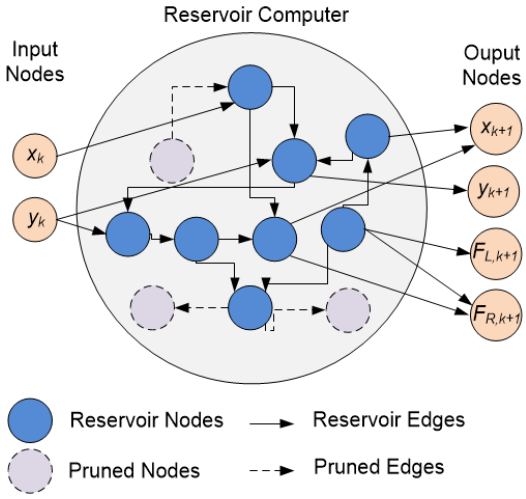

Figure 3: An overview of the truncated reservoir computing framework with initial random connectivity, developed for simulating the dynamical behaviour of the bipedal SLIP model. The reservoir input is the coordinates of the mass M at the time step t_k, and the reservoir output is the same coordinates at the next time step along with the ground reaction forces of the left and right legs. Pruned nodes and edges are shown with dashed lines and circles.

Given the above computational framework, noisy body coordinates corresponding to the time step $t_k = k\Delta t$ are used as the input data, i.e., $\mathbf{u}_k = [\tilde{x}_k \;\; \tilde{y}_k\;]^T$ to predict the motion at the next time step $t_{k+1} = (k+1)\Delta t$, producing $\mathbf{y}_{k+1} = \left[x_{k+1} \;\; y_{k+1} \;\; F_{L,k+1} \;\; F_{R,k+1}\right]^T$ as the system output, where $F_{L,k+1}$ and $F_{R,k+1}$ are the left and right legs' vertical reaction forces. A by-product of this prediction is the vertical ground reaction forces of the left and right legs. However, training the reservoir and its hyperparameters requires establishing a suitable data set containing potential periodic motions. For this purpose, we first train the reservoir, optimise its hyperparameters, and remove redundant nodes and edges, using simple walking and running motions, as shown in Figure 2. Then, we examine whether it works for held-out data sets. Based on the above explanations, Figure 4 provides a flowchart representing the computational protocol developed for training and testing reservoir computers using noisy locomotion dynamics.

4 RESULTS AND DISCUSSION

4.1 Description of Assumptions and Data

Based on the bipedal SLIP model presented earlier, a set of synthetic data is generated representing a combination of walking and running motions. This data set is around 0.73 s long, sampled at 31.7 kHz. The first half segment of this data set is used for the training, and the second half segment is held out as a validation set. Two cases are considered: noise-free data and Gaussian white noise-contaminated data. Figure 4 shows the time series of the coordinates and the vertical ground reaction forces, where those curves labelled as ground truth represent the noise-free generated data.

Proceedings of ACOUSTICS 2025
12-14 November 2025,
Joondalup, Australia

The reservoir computer is initialised with 800 randomly connected neurons. Then, based on the training data, the readout matrix is identified using Eq. (7). For this initial reservoir computer, the mean-squared error (MSE) is evaluated for the validation set and shown in Figure 5. Hyperparameters are next optimised to produce a tuned reservoir. The method appeared in Sedehi et al. (2025) is employed here, which requires prescribing the initial boundaries for a holistic search, as given below:

$$\begin{cases} \alpha \in [0.01, 1.00] \\ \zeta \in [0.01, 1.00] \\ \beta \in [0.01, 2.00] \\ p \in [0.1, 0.9] \end{cases} \tag{8}$$

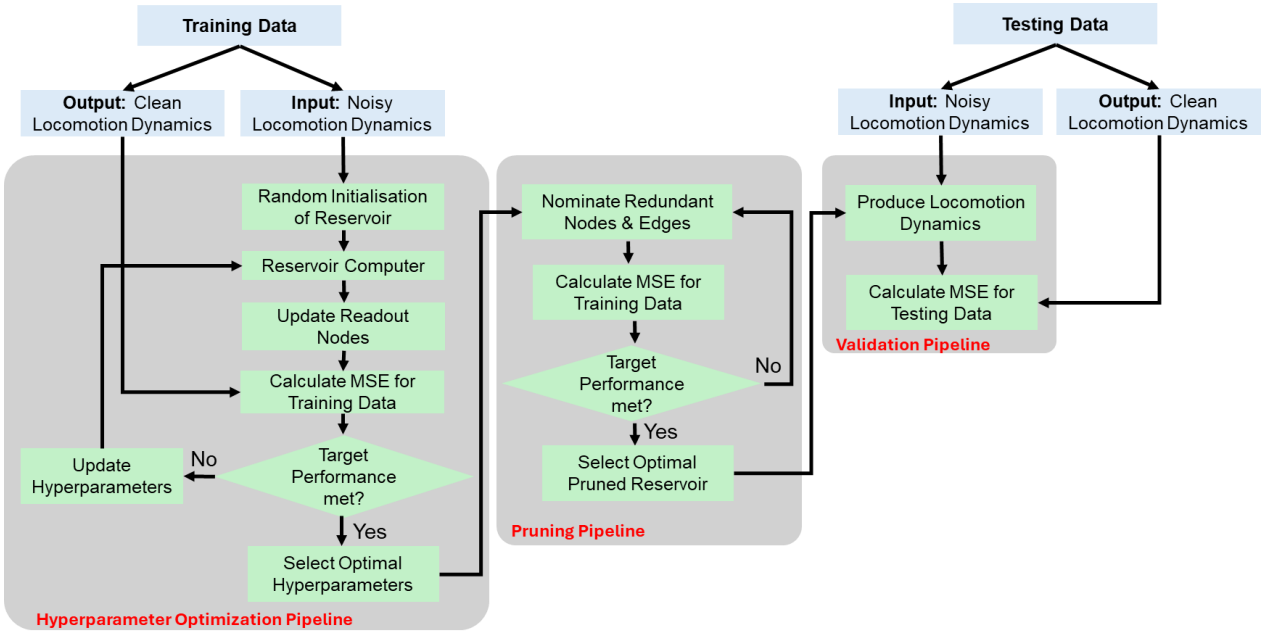

Figure 4: Computational protocol developed for training and testing of truncated reservoir computers. The method comprises three major components, including hyperparameter optimisation, pruning redundant nodes and edges, as well as validation pipelines.

Note that the ridge coefficient (λ) is selected separately during each re-estimation of the readout matrix. By doing so, the explicit solution of Eq. (7) remains valid, avoiding extra computational complexity.

Pruning of the reservoir neurons and synapses is carried out using the framework explained earlier. The tuned reservoir is thus further refined by removing several ineffective neurons. However, performing the pruning requires a pre-selection strategy to identify those neurons and synapses that minimally contribute to the prediction accuracy to be able to rank them accordingly. Intuitively speaking, synapses with larger weights in the reservoir matrix should be more important to the reservoir performance, and neurons with more important synapses are seemingly more necessary. Another criterion to select redundant neurons is the absolute mean and variance of the nodal states, which can represent whether the corresponding neurons are active over the training time. In effect, larger absolute mean and variance of neuronal states can show greater activity and importance to the performance. Finally, the number of incoming and outgoing synapses to a neuron can indicate greater involvement and importance to the reservoir performance compared to those neurons with few to no connectivity to the reservoir's input and output.

After identifying potential neurons and synapses for removal, the validation accuracy is computed without the nominated neurons, and if beneficial, they are removed. This process continues until either a pre-selected target for performance improvement is achieved or the maximum number of pruned neurons is reached. In this study, for simplicity, the latter criterion is used considering one hundred iterations.

4.2 Case I: Noise-free Data

For noise-free data, when the loss function in Eq. (6) is optimised for the hyperparameters, the optimal values are obtained as $\hat{\alpha} = 0.01$, $\hat{\zeta} = 1.00$, $\hat{\beta} = 2.00$, and $\hat{p} = 0.9$. As shown in Figure 6, the MSE is significantly smaller for the tuned reservoir when compared to the initial reservoir, and this result further highlights the essence of proper calibration of the reservoir computer and its hyperparameters. Figure 6 also compares the validation accuracy of the pruned reservoir with the tuned and pruned ones. Although around eighty nodes are removed using the pruned

reservoir, its performance is somewhat equivalent to the tuned reservoir and still much better than the initial reservoir. Figure 5 compares the time series of the predictions made by the pruned reservoir compared to the ground truth data, emphasising the validity and accuracy of the presented method.

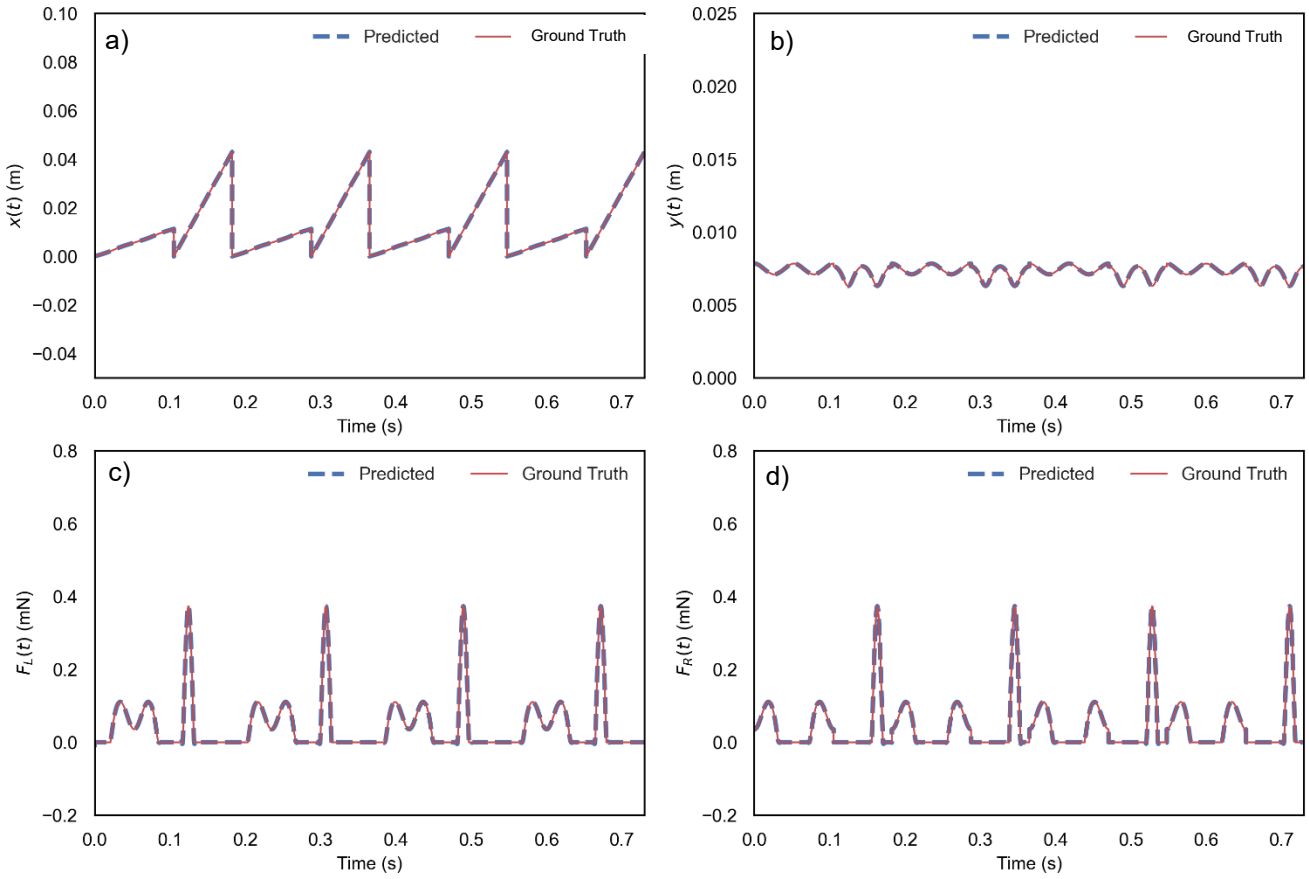

Figure 5: Predictions of the coordinates and the vertical reaction forces using the pruned reservoir computer when no measurement noise is present: (a) The horizontal component of the motion (b) The vertical component of the motion (c) Vertical reaction force of the left leg (d) Vertical reaction force of the right leg. In all plots, the dashed blue colour curves show the predictions, and the red colour curves show the ground truth.

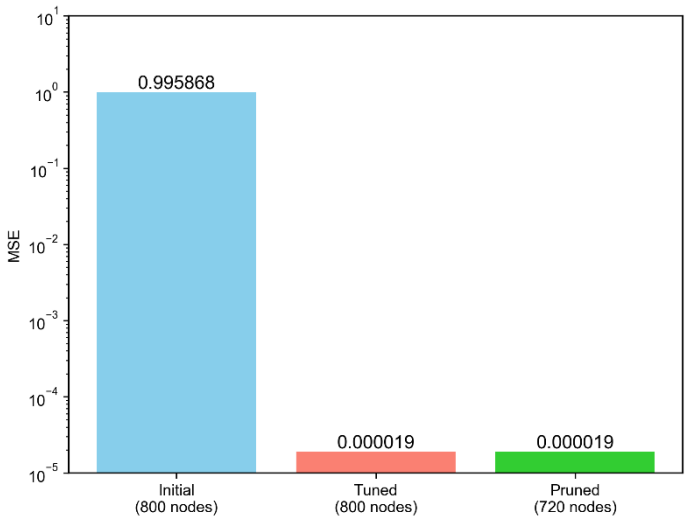

Figure 6: Comparison of prediction errors for the initial reservoir started with connectivity, the tuned reservoir obtained via hyperparameter optimisation, and the pruned reservoir generated via removing eighty nodes and related edges.

Proceedings of ACOUSTICS 2025
12-14 November 2025,
Joondalup, Australia

Figure 7 shows the contour plots of the normalised MSE for the joint space of the leakage rate and the spectral radius. The optimum point is recognised as very close to the boundary specified for the hyperparameters, i.e., $\hat{\alpha} = 0.01$ and $\hat{\zeta} = 1.00$. This result was expected due to the noise-free nature of the data, which leads to obtaining a small value for the leakage rate, suggesting that the correlation between consecutive steps of the reservoir states remains the most relevant for one-step-ahead predictions. Conversely, the reservoir dynamics have subtle contributions to the output due to the small leakage rate.

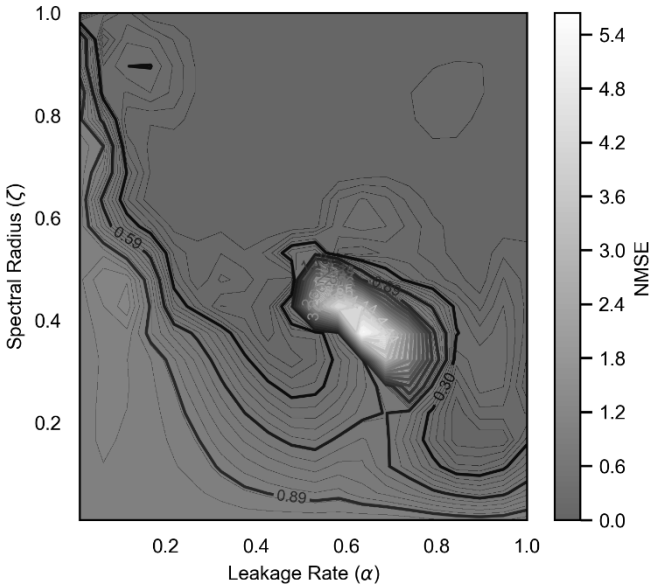

Figure 7: Identification of the leakage rate and the spectral radius when considering no measurement noise. The optimal point is $\hat{\alpha} = 0.01$ and $\hat{\zeta} = 1.00$.

4.3 Case II: Noisy Data

This section shows results on case II, where additive GWN is super-imposed on the training data with a standard deviation equal to 25% root-mean-square of the noise-free signals (SNR = 12.04 dB). Similar to the preceding case, an initial reservoir computer is generated, and then, hyperparameter optimisation and pruning are carried out. Figure 8 compares the accuracy of initial, tuned, and pruned reservoirs, showing significant improvement in the MSE for the reservoir whose hyperparameters are tuned, and its redundant nodes are discarded.

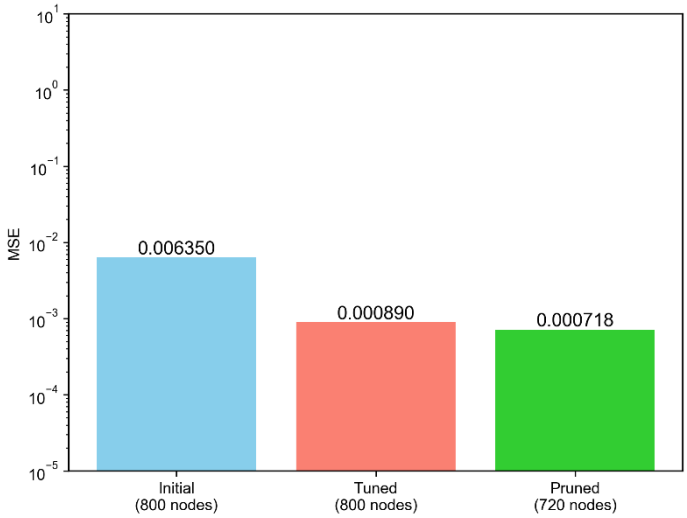

Figure 8: Comparison of prediction errors for the initial reservoir started with random connectivity, the tuned reservoir obtained via hyperparameter optimisation, and the pruned reservoir generated via removing 80 nodes and related edges.

Figure 9 compares the predictions of the coordinates and vertical ground reaction forces for the left and right legs obtained using the pruned reservoir. The presented reservoir discards a significant amount of noise from the data and provides accurate predictions with reduced computational costs.

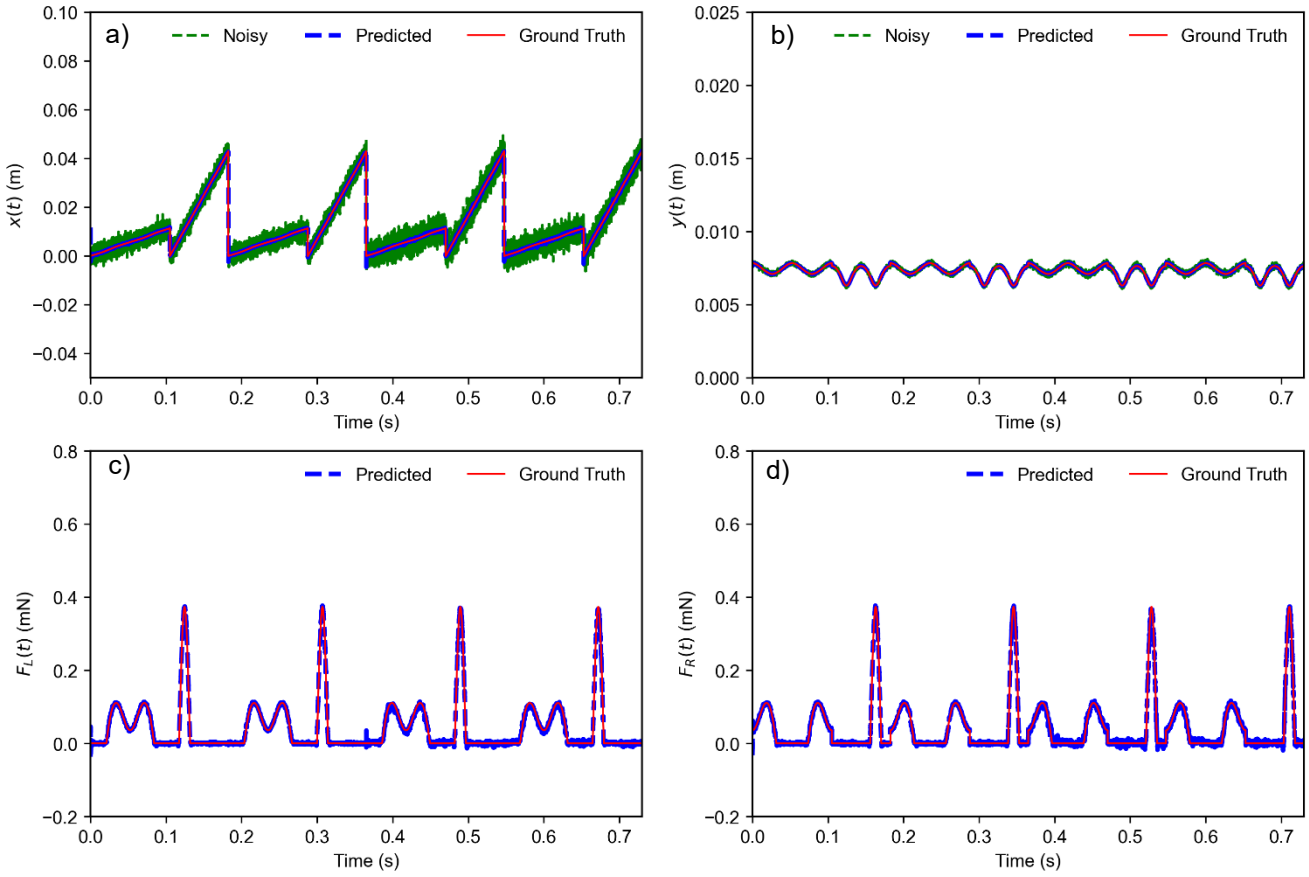

Figure 9: Predictions of the coordinates and the vertical reaction forces using the pruned reservoir computer when 25% root-mean-square additive GWN is present: (a) The horizontal component of the motion (b) The vertical component of the motion (c) Vertical reaction force of the left leg (d) Vertical reaction force of the right leg. In all plots, the dashed blue colour curves show the predictions, and the red colour curves show the ground truth.

The contours of the normalised MSE are shown in Figure 10 for the joint space of the leakage rate and spectral radius when the noisy data is used for the training and optimisation. The optimal leakage rate and the spectral radius are obtained as $\hat{\alpha} = 0.14$ and $\hat{\zeta} = 0.89$. The high value of the leakage rate indicates substantial contributions of the reservoir dynamics in predicting the locomotion states and the ground reaction forces. Due to the presence of noise, the incremental correlation between the reservoir states has a limited contribution to reproducing the nonlinear dynamics of the bipedal SLIP model.

5 COMPARISON WITH ALTERNATIVE NEURAL ARCHITECTURES

ESN-based reservoir computers are often classified as a special form of recurrent neural networks, covering a wide range of configurations. However, a significant difference between the ESN and other recurrent neural networks lies in the computational approaches used for calibrating network parameters. As presented, the training of the reservoir computers is founded upon ridge regression, offering a closed-form gradient-free expression for updating the readout nodes. This approach is computationally efficient and does not involve calculating network gradients. However, when the hyperparameter optimisation and pruning are applied, the computational cost will inherently increase in exchange for performance improvement. In contrast, other network architectures are founded upon the gradient-based optimisation techniques, which may lead to exploding or diminishing gradients, especially when dealing with time series with many data points (Zucchet & Orvieto, 2024). As a result, the training of recurrent networks on nonlinear dynamics problems often encounters computational difficulties due to the gradient calculation. Notably, a numerical comparison with such networks is an interesting subject, but it is left to be

studied in the future in view of the length of the paper, as it involves leveraging a wide range of technical details that differ from those of reservoir computers.

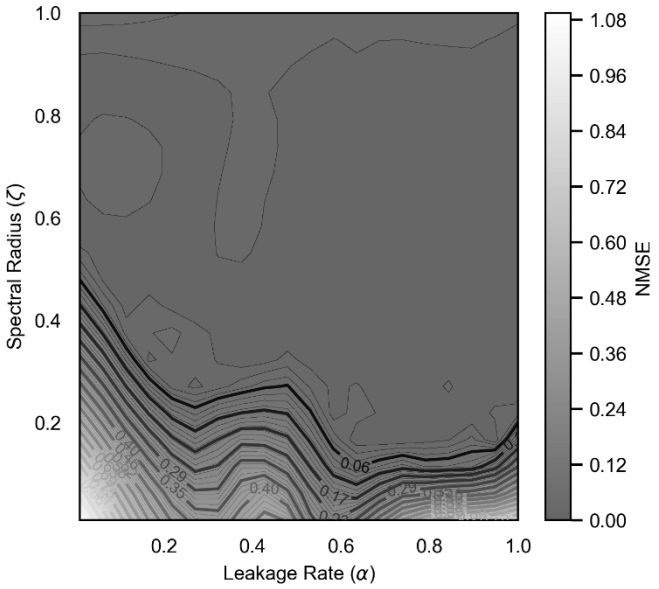

Figure 10: Identification of the leakage rate and spectral radius when considering 25% root-mean-square measurement noise. The optimal point is $\hat{\alpha} = 0.14$ and $\hat{\zeta} = 0.89$.

6 CONCLUSIONS

A reservoir computer framework is presented for reproducing the nonlinear dynamics of the bipedal SLIP model, representing insect locomotion. Optimisation of the hyperparameters is addressed through the minimisation of the loss function of a training data set, and pruning of the reservoir nodes and edges is addressed via introducing a few metrics for nominating the less effective or unnecessary structures. As a result, one-step-ahead predictions of the coordinates and the vertical ground reaction forces are obtained from noisy records of the coordinates of the mass centre. Results show remarkable accuracy in the predictions of the reservoir. Comparing with the conventional reservoir computer approaches where random connectivity and hyperparameter selection are exercised for predictions, the presented tuned and pruned reservoir computers demonstrate improvement in the MSE indices up to several orders of magnitude. While synthetic data is employed herein for examining the viability of the concept and implementation of the reservoir computers, our future works will potentially demonstrate the method with real measurements from ants' and termites' walks. Such developments are also important in terms of studying the locomotion mechanisms in small arthropods, unveiling further applications for termite control via hardware implementation of predator cues or prey feeding signals.

ACKNOWLEDGEMENTS

This research was supported under the Australian Research Council's (ARC) Linkage funding scheme project No. LP200301196.

REFERENCES

Blickhan, R., & Full, R. J. (1993). Similarity in multilegged locomotion: bouncing like a monopode. Journal of Comparative Physiology A, 173(5), 509-517.

Evans, T. A., Lai, J. C., Toledano, E., McDowall, L., Rakotonarivo, S., & Lenz, M. (2005). Termites assess wood size by using vibration signals. *Proceedings of the National Academy of Sciences*, *102*(10), 3732-3737.

Full, R. J., Blickhan, R., & Ting, L. H. (1991). Leg design in hexapedal runners. Journal of Experimental Biology, 158(1), 369-390.

Full, R. J., & Tu, M. S. (1990). Mechanics of six-legged runners. *Journal of experimental biology*, *148*(1), 129-146.

Gan, Z., Yesilevskiy, Y., Zaytsev, P., & Remy, C. D. (2018). All common bipedal gaits emerge from a single passive model. *Journal of The Royal Society Interface*, *15*(146), 20180455.

Gan, Z., Jiao, Z., & Remy, C. D. (2018). On the dynamic similarity between bipeds and quadrupeds: a case study on bounding. *IEEE Robotics and Automation Letters*, *3*(4), 3614-3621.

Geyer, H., Seyfarth, A., & Blickhan, R. (2006). Compliant leg behaviour explains basic dynamics of walking and running. Proceedings of the Royal Society B: Biological Sciences, 273(1603), 2861-2867.

Ghani, A., McGinnity, T. M., Maguire, L., McDaid, L., Belatreche, A., & Shabtai, N. (2010). Neuro-inspired speech recognition based on reservoir computing. *Advances in Speech Recognition*, *164*, 50.

Inta, R., Lai, J.C.S., Fu, E.W. & Evans, T.A. (2007). Termites live in a material world: exploration of their ability to differentiate between food sources. *J. R. Soc. Interface*, 15, 735-44.

Jaeger, H., & Haas, H. (2004). Harnessing nonlinearity: Predicting chaotic systems and saving energy in wireless communication. Science, 304(5667), 78-80.

Oberst, S., Lai, J.C.S. & Evans, T.A. (2016). Termites utilise clay to build structural supports and so increase foraging resources. Scientific Reports, 6, 20990.

Oberst S, Lai JCS & Evans TA (2019) “Physical Basis of Vibrational Behavior – Channel Properties and Noise”, in *Biotremology: Studying Vibrational Behavior*, Springer International Publishing, Heidelberg New York, Germany. ISBN 978-3-030-22292-5. http://dx.doi.org/10.1007/978-3-030-22293-2

Oberst, S., Bann, G., Lai, J. C., & Evans, T. A. (2017). Cryptic termites avoid predatory ants by eavesdropping on vibrational cues from their footsteps. *Ecology Letters*, *20*(2), 212-221.

Oberst, S., Lenz, M., Lai, J. C., & Evans, T. A. (2019). Termites manipulate moisture content of wood to maximize foraging resources. *Biology Letters*, *15*(7), 20190365.

Oberst, S., Tofigh, F., Lai, J., Mankowski, M., Arango, R., & Kirker, G. (2025). Development of a micro-exciter to mimic insect vibration signals and the effect of the substrate on the playback response. *The Journal of the Acoustical Society of America*, *157*(4_Supplement), A186-A186.

Oberst, S., Lai, J. C. S., (2025). A mixed SLIP-BSLIP walking model with uncertainty to mimic insect ground reaction forces” The 31st International Congress on Sound and Vibration (ICSV31), Incheon, South Korea.

Pelit, M. M., Chang, J., Takano, R., & Yamakita, M. (2020, July). Bipedal walking based on improved spring loaded inverted pendulum model with swing leg (slip-sl). In 2020 IEEE/ASME International Conference on Advanced Intelligent Mechatronics (AIM) (pp. 72-77).

Ren, B., & Ma, H. (2022). Global optimization of hyper-parameters in reservoir computing. *Electronic Research Archive*, *30*(7).

Reinhardt, L., Weihmann, T., & Blickhan, R. (2009). Dynamics and kinematics of ant locomotion: do wood ants climb on level surfaces? Journal of Experimental Biology, 212(15), 2426-2435.

Sansom, T. M., Lai, J.C.S., Halkon, B., Evans, T. A., Oberst, S., (2025). Termite vibration sensing: the chordotonal organs and their appendages, Ecology and Evolution (under-review).

Sedehi, O., Yadav, M., Stender, M., & Oberst, S. (2025). Denoising and Reconstruction of Nonlinear Dynamics using Truncated Reservoir Computing. *Chaos* 35 (9): 093103.

Seidl, T., & Wehner, R. (2008). Walking on inclines: how do desert ants monitor slope and step length. Frontiers in zoology, 5(1), 8.

Thorne, B., Jüngling, T., Small, M., Corrêa, D., & Zaitouny, A. (2022). Reservoir time series analysis: Using the response of complex dynamical systems as a universal indicator of change. *Chaos: An Interdisciplinary Journal of Nonlinear Science*, *32*(3).

Yadav, M., Sinha, S., & Stender, M. (2025). Evolution beats random chance: Performance-dependent network evolution for enhanced computational capacity. *Physical Review E*, *111*(1), 014320.

Zucchet, N., & Orvieto, A. (2024). Recurrent neural networks: vanishing and exploding gradients are not the end of the story. *Advances in Neural Information Processing Systems*, *37*, 139402-139443.